Available online at www.sciencedirect.com
ScienceDirect
Journal of the European Ceramic Society 27 (2007) 377–388
www.elsevier.com/locate/jeurceramsoc

Degradation mechanisms of a SiC fiber reinforced self-sealing matrix composite in simulated combustor environments

Ludovic Quemard [a], Francis Rebillat [a,*], Alain Guette [a], Henri Tawil [b], Caroline Louchet-Pouillerie [b]

[a] *Laboratoire des Composites Thermostructuraux, UMR 5801 (CNRS-SAFRAN-CEA-UB1), 3 Allée de la Boétie, 33600 Pessac, France*
[b] *Snecma Propulsion Solide, Les Cinq Chemins, 33187 Le Haillan, France*

Received 23 November 2005; received in revised form 10 February 2006; accepted 17 February 2006
Available online 26 May 2006

Abstract

Non-oxide ceramic matrix composites are potential candidates to replace the current nickel-based alloys for a variety of high temperature applications in the aerospace field. The durability of a $SiC_{(f)}/PyC_{(i)}/[Si, C, B]_{(m)}$ composite with a multi-layered self-sealing matrix and Hi-Nicalon fibers was investigated at 1200 °C for exposure durations up to 600 h. The specimens are aged in a variety of slow-flowing air/steam gas mixtures and total pressures, ranging from atmospheric pressure with a 10–50% water content to 1 MPa with 10–20% water content. The degradation of the composite was determined from the measurement of residual strength and strain to failure on post-exposure specimens and correlated with microstructural observation of the damaged tows. The most severe degradation of the composite occurred at 1 MPa in an air/steam (80/20) gas mixture. Correlation between this degradation and the dissolving of the SiC fibers in the generated boria-containing glass, is discussed.

Keywords: Ceramic matrix composites; Corrosion; Mechanical properties; Lifetime; Engine components; SiC fibers

1. Introduction

Non-oxide ceramic matrix composites such as $SiC_{(f)}/PyC_{(i)}/SiC_{(m)}$ consist of SiC matrix reinforced with SiC fibers and pyrocarbon (PyC) interfacial coating. These composites exhibit a low density associated with high thermomechanical properties and are potential candidates to replace the current nickel-based alloys for a variety of long-term applications in the aerospace field. In these applications, $SiC_{(f)}/PyC_{(i)}/SiC_{(m)}$ components can be subjected to service conditions that include mechanical loading under intermediate to high temperatures and high pressure complex environment containing oxygen and steam. The oxidation of the PyC weak interphase can occur under dry air at a temperature lower than 500 °C and leads to interfacial degradations of $SiC_{(f)}/PyC_{(i)}/SiC_{(m)}$. $SiC_{(f)}/PyC_{(i)}/[Si, C, B]_{(m)}$ composites with a sequenced self-sealing matrix have been developed[1,2] and investigated[3–11] to protect the PyC interphase against oxidation effects up to 1400 °C. The principles of the self-sealing approach are to consume part of the incoming oxygen and limit access of residual oxygen to the PyC interphase by sealing the matrix microcracks with a SiO_2–B_2O_3 oxide phase. However, previous studies showed that B_2O_3[4–6,8,12,13] and SiO_2[15,17] can volatilize, respectively, at 600 and 1100 °C under water vapor-containing environments. This phenomenon can cause the self-sealing capability to degrade, thus reducing the lifetime of the $SiC_{(f)}/PyC_{(i)}/[Si, C, B]_{(m)}$.

The matrix layers are SiC, B_4C and a phase noted Si–B–C. The efficiency of the self-sealing process under environments containing both oxygen and water vapor, results from the competition between the oxidation of the matrix layers and the volatilization of the generated oxide phase.

Under dry air, B_4C undergoes oxidation and volatilization reactions below 600 and 900 °C, respectively, as shown below[4–6,8,12,13]:

$$B_4C_{(s)} + 4O_{2(g)} = 2B_2O_{3(l)} + CO_{2(g)} \quad (1)$$

$$B_2O_{3(l)} = B_2O_{3(g)} \quad (2)$$

Under water vapor-containing environments, $B_2O_{3(l)}$ may react significantly at 600 °C to form hydroxydes by the following

* Corresponding author. Fax: +33 5 56 84 12 25.
E-mail address: rebillat@lcts.u-bordeaux1.fr (F. Rebillat).

0955-2219/$ – see front matter © 2006 Elsevier Ltd. All rights reserved.
doi:10.1016/j.jeurceramsoc.2006.02.042

reactions[4–6,8,12,13]:

$$\frac{3}{2}B_2O_{3(l)} + \frac{3}{2}H_2O_{(g)} = H_3B_3O_{6(g)} \quad (3)$$

$$\frac{3}{2}B_2O_{3(l)} + \frac{1}{2}H_2O_{(g)} = H_3BO_{3(g)} \quad (4)$$

$$\frac{1}{2}B_2O_{3(l)} + \frac{1}{2}H_2O_{(g)} = HBO_{2(g)} \quad (5)$$

The competition between the oxidation (1) and volatilization reactions (2)–(5) can lead to the recession of B_4C.

In high temperature environments and under dry air, the active oxidation of SiC occurs above 1000 °C and below $P_{O_2} = 100$ Pa according to (6). At a higher P_{O_2}, a paralinear oxidation of SiC[14] occurs to form a protective SiO_2 scale according to (7). In environments containing O_2 and H_2O, the formation of SiO_2 is dramatically enhanced by reaction (8)[14–16]:

$$SiC_{(s)} + O_{2(g)} = SiO_{(g)} + CO_{(g)} \quad (6)$$

$$2SiC_{(s)} + 3O_{2(g)} = 2SiO_{2(s)} + 2CO_{(g)} \quad (7)$$

$$SiC_{(s)} + 3H_2O_{(g)} = SiO_{2(s)} + CO_{(g)} + 3H_{2(g)} \quad (8)$$

Under steam-containing environments, the SiO_2 scale may volatilize, by the main following reaction[17]:

$$SiO_{2(s)} + 2H_2O_{(g)} = Si(OH)_{4(g)} \quad (9)$$

The volatilization rate of SiO_2[15,17] is much lower than for B_2O_3.[4–6,8,12,13] However, as for boron matrix layers, the competition between the oxide formation (7) and (8) and the oxide phase volatilization (9) reactions can lead to the recession of SiC.[18–20]

The Si–B–C matrix layer can be described as a mixture of SiC nanocrystals in an amorphous B_4C phase.[7] A previous study investigated the oxidation of Si–B–C coatings under oxygen and steam-containing environments by thermogravimetric analysis.[4,5] It has been shown that SiC nanocrystals can oxidize significantly at 600 °C and at atmospheric pressure, simultaneously to the B_2O_3 formation, to form silica according to reaction (7).

Previous works[9] focused on the corrosion behavior of the $SiC_{(f)}/PyC_{(i)}/[Si, C, B]_{(m)}$ at high pressure and at 600 °C. The aim of this study is to evaluate, at a higher temperature, the effects of both oxygen and water vapor on the self-sealing process of $SiC_{(f)}/PyC_{(i)}/[Si, C, B]_{(m)}$ composites subjected to high-pressure environments. Corrosion tests are conducted for long periods of time on $SiC_{(f)}/PyC_{(i)}/[Si, C, B]_{(m)}$ composites at 1200 °C in oxygen and steam-containing environments at atmospheric pressure and high pressure. Post-exposure mechanical tests are performed at room temperature (RT) to investigate the effects of corrosion phenomena on the retained mechanical properties.

2. Materials and test specimens

The material investigated is the CERASEP® A410[10,11] (C410) manufactured by Snecma Propulsion Solide (France) via chemical vapor infiltration (CVI). It is a woven-SiC-fiber reinforced [Si, C, B] sequenced matrix composite (Fig. 1). The

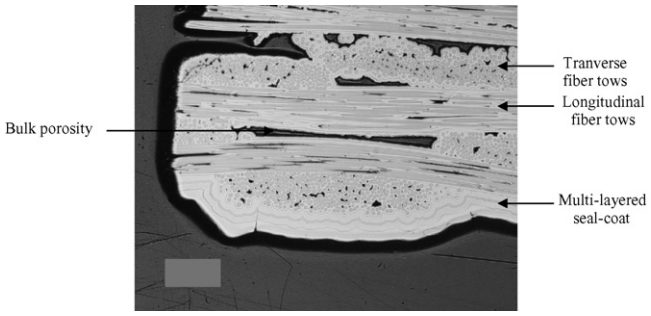

Fig. 1. Polished cross-section of the as-received C410 material.

different matrix layers are crystallised SiC, amorphous B_4C and a SiC–B_4C phase named Si–B–C which can be described as a mixture of SiC nanocrystals in a B_4C amorphous phase.[7] The sequenced matrix is reinforced by Hi-Nicalon® SiC fibers and plane multi-layer reinforcement is used to eliminate delamination sensitivity that is common for 2D ceramic matrix composites. Fiber volume fraction, material density and mainly closed bulk porosity, as reported by the composite manufacturer, are, respectively, 34%, 2.25 ± 0.05 and 13 ± 1%. The interphase is pyrocarbon.

The test specimen geometry used in this study has a reduced gauge section (Fig. 2). It is 200 mm long, with a grip section width of 24 mm, a reduced gauge section width of 16 mm and a thickness of 4.4 mm. Two different material batches, manufactured in similar conditions, are used for these works. Test samples are machined from composite plates using diamond grinding and then are seal-coated with CVI layers of SiC, B_4C and Si–B–C. The sequenced seal-coat thickness, with a SiC final layer, is 120 μm on the composite surface and about 40 μm on the machined edges. Corrosion tests are also performed on Si–B–C coating and SiC/SiC coupons for comparison purposes. The Si–B–C coating, with a thickness of 30 ± 3 μm, is deposited on SiC chips (diameter of 8 mm and thickness of 2 mm) via chemical vapor deposition (CVD).

3. Test procedures

3.1. Pre-damaging

The dog-bone specimens are loaded in tension monotonically at room temperature to a tensile stress of 150 MPa (the stress cor-

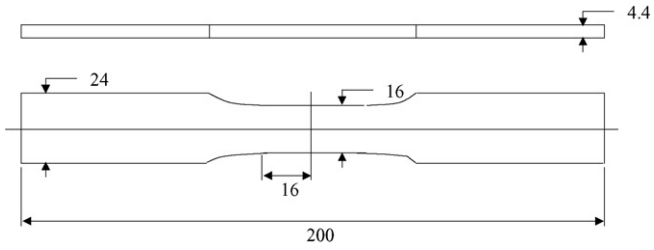

Fig. 2. C410 specimen geometry used in this study. Dimensions are in millimeters.

Table 1
Summary of the test conditions for C410 composites exposed at 1200 °C in various environments

No.	Exposure	T (°C)	P_{Tot} (MPa)	Air/steam	P_{O_2} (kPa)	P_{H_2O} (kPa)	P_{H_2O}/P_{O_2}	v (cm s^{-1})
A	Furnace	1210 ± 10	0.1	90/10	18	10	0.56	5
B	Furnace	1210 ± 10	0.1	80/20	16	20	1.25	5
C	Furnace	1200 ± 15	0.1	50/50	10	50	5	10
D	HP furnace	1220 ± 25	0.45	90/10	81	45	0.56	8
E	HP furnace	1225 ± 30	1	90/10	180	100	0.56	8
F	HP furnace	1225 ± 30	1	80/20	160	200	1.25	8

responding to twice their elastic limit) then unloaded before the corrosion exposures. The aim of this pre-damaging is to generate a controlled crack network in the matrix, which facilitates the ingress of the corrosive species. The residual strain is very low (≅0.001%) and can be neglected for post-exposure mechanical tests. The pre-damaging microcracks are mainly located in the seal-coat of the gauge section of the specimens. At room temperature, their mean spacing distance is 230 ± 30 μm and their width is 0.5–3 μm. In addition, few microcracks with a width lower than 1 μm at RT are present at the edge of the macroporosities.

3.2. Corrosion tests

The corrosion test conditions are reported in Table 1. Two corrosion test equipments are used for these tests. High pressure corrosion tests are conducted in the high pressure–high temperature furnace[21] (Fig. 3). High pressure air is provided by a pressurized gas supply system then mixed with water in an evaporator. The air and water flows are independently controlled by mass flow meters and the air/H_2O gas mixture is injected in the alumina test tube (i.d.: 34 mm, purity: 99.7%, OMG, France) of the furnace. A system of pneumatically driven back pressure

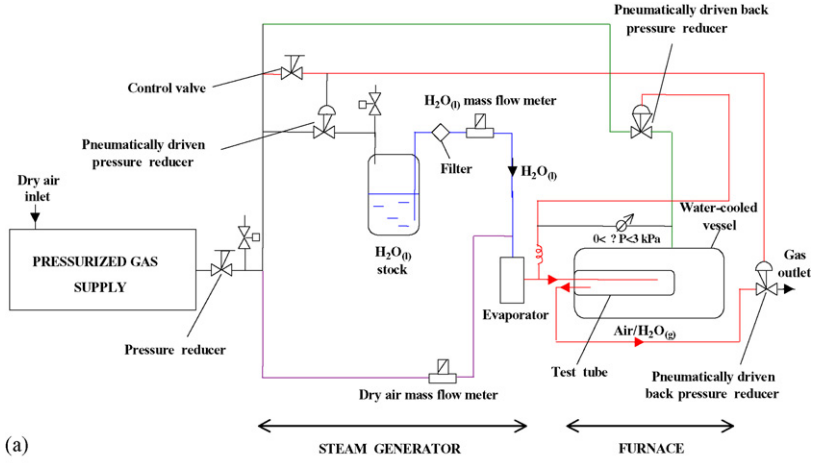

Fig. 3. Schematic of the high temperature–high pressure corrosion test equipment (a) and view of the furnace (b).

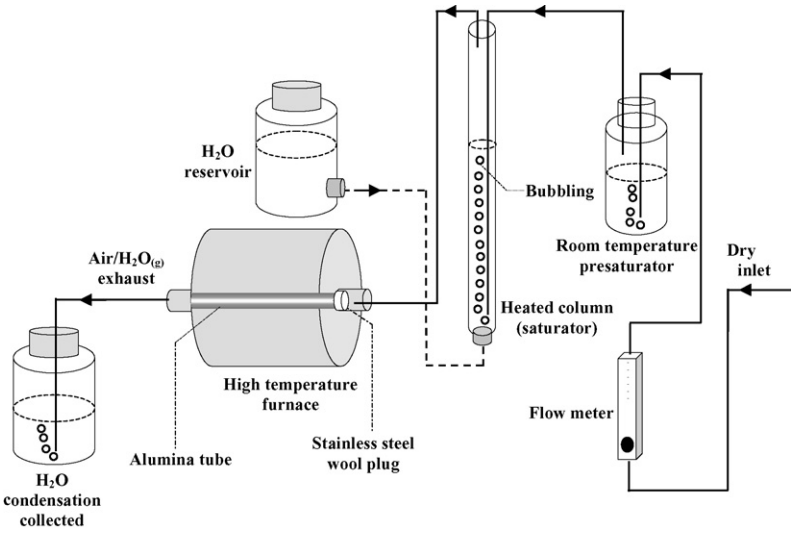

Fig. 4. Schematic of the high temperature furnace and the water vapor saturator at atmospheric pressure.

reducers maintains a slight difference of pressure between the tube interior and the metallic vessel ($P_{tube} - P_{vessel} = -3$ kPa). This permits to minimize stresses on the tube and increase its airtightness. The uniform heating zone of the furnace is approximately 120 mm long which is longer than the gage length of the specimens.

A high temperature furnace associated with a water saturator is used to run the corrosion tests at atmospheric pressure (Fig. 4). The dry air flows through a heated water column in order to be saturated in steam before its introduction in the alumina tube (i.d.: 34 mm, purity: 99.7%, OMG, France) of the furnace. The temperature of the water in the column is slightly higher than the dewpoint corresponding to the desired water vapor partial pressure. For example, an air/steam (90/10) gas mixture is obtained for a column temperature of 48 °C (dewpoint for $P_{H_2O} = 10$ kPa is 46 °C). Water content in the gas stream is monitored by measuring the condensate in the gas exhaust daily and the amount of water in the stock which supplies the heated column. The uniform heating zone of the furnace is approximately 220 mm long.

In both corrosion test equipments, the C410 specimens are oriented parallel to the gas flow and placed on alumina sample holders (purity: 99.7%, OMG, France) specially designed. The heating and cooling rates, used at atmospheric pressure under ambient air, are, respectively, 150 and 100 °C h^{-1}. The exposures are regularly interrupted to weigh the specimens using a scale (Precisa Instruments AG, Switzerland) with an accuracy of 1×10^{-2} mg.

3.3. Characterization of specimens after exposure

Post-exposure cyclic tensile tests are performed at RT on the dog-bone specimens. A spring-loaded clip on-gauge is attached to the 25 mm long of the straight section of the samples to record displacement. The composites are tested up to failure in a servo controlled testing machine (INSTRON 1185) equipped with self aligning grips at a cross-head speed of $0.40 \pm 0.05\%$ min^{-1}.

After exposures, the test specimens are cut perpendicularly and parallel to the loading axis then polished for examination using an optical microscope. Moreover, the fractured surfaces are analyzed by scanning electron microscopy (SEM). The chemical composition of the oxide phase formed during the corrosion tests is determined on polished cross-sections of the composites using electron probe micro analysis (EPMA, CAMECA SX100).

4. Results

4.1. Post-exposure mechanical results

The post-exposure mechanical properties of the C410 predamaged specimens are determined using cyclic tensile tests at RT. The results are shown in Fig. 5 and reported in Table 2. Three C410 specimens are used to determine the mechanical properties up to failure of the two batches of the as-received material using cyclic tensile tests at RT.

The failures of all the specimens occurred in the gauge section. Small brittle rupture areas and wide non-brittle rup-

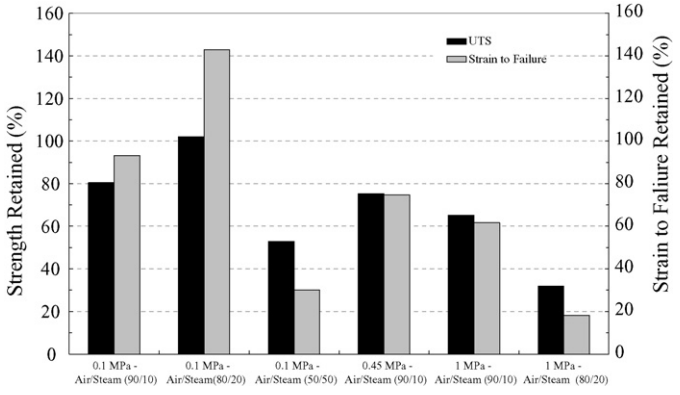

Fig. 5. The effect of corrosion environments on the ultimate strength and on the strain to failure of the C410 specimens exposed for 600 h.

Table 2
Summary of C410 composites post-exposure tensile properties at RT

Test condition	Batch	Exposure time (h)	Weight change (%)	Failure	UTS (MPa)	Strain to failure (%)	*E* (GPa)
A	2	611	+3.4	B areas[a]	296	0.68	170
B	1	616	+2.4	B areas	310	0.65	220
C	2	601	+3.3	B[b]	195	0.22	220
D	1	606	+4.4	B	229	0.34	210
E	2	609	+3.9	B	240	0.45	170
F	1	603	+5.9	B	97	0.08	180
As-received (average)	1	–	–	NB[c]	304 ± 45	0.46 ± 0.12	252 ± 4
As-received (average)	2	–	–	NB	368 ± 11	0.73 ± 0.02	186 ± 21
C410 data base[15,16]		–	–	NB	315 ± 20	0.5	220 ± 25

[a] Presence of brittle rupture areas.
[b] Brittle rupture.
[c] Non-brittle rupture.

ture areas characterized by fiber pull-out, are observed on the fractured surfaces (Fig. 6) of the specimens exposed in low steam-pressure environments (conditions A and B). Brittle rupture areas are located at the edge of the bulk porosities filled with an oxide phase. The stress–strain curves of the specimens tested in low steam-pressure environment are similar to the as-received ones (Fig. 7). Thus, a non-linear stress–strain behavior without a plateau is observed up to the ultimate failure of the specimens. According to this behavior induced by matrix cracking, a continuous damaging occurred in the composite up to its failure. Moreover, the width of the hysteresis loops is narrow and the residual strains after unloading are very low. This indicates a high fiber–matrix load transfer, thus a strong interfacial shear stress. The retained mechanical properties of samples aged at low steam-pressure are similar to the as-received materials and C410 data base,[10,11] indicating that the fibers are not damaged significantly (Fig. 5). Many brittle rupture areas, located

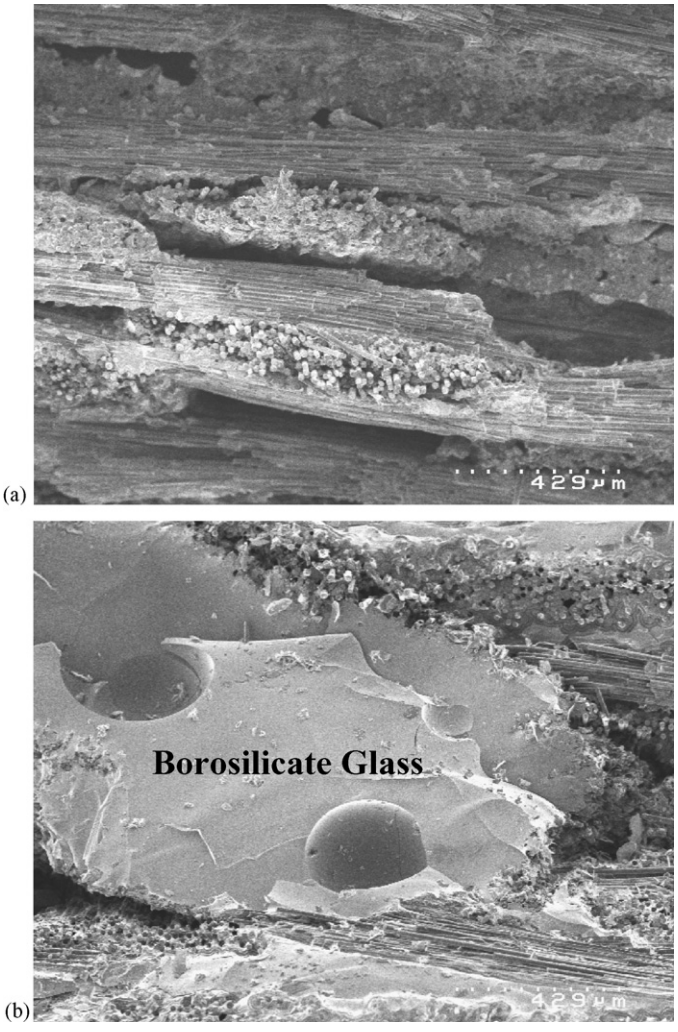

Fig. 6. SEM fracture surfaces of C410 specimens exposed in an air/steam (80/20) gas mixture for 616 h at 1200 °C and 0.1 MPa (a) and for 603 h at 1200 °C and 1 MPa (b).

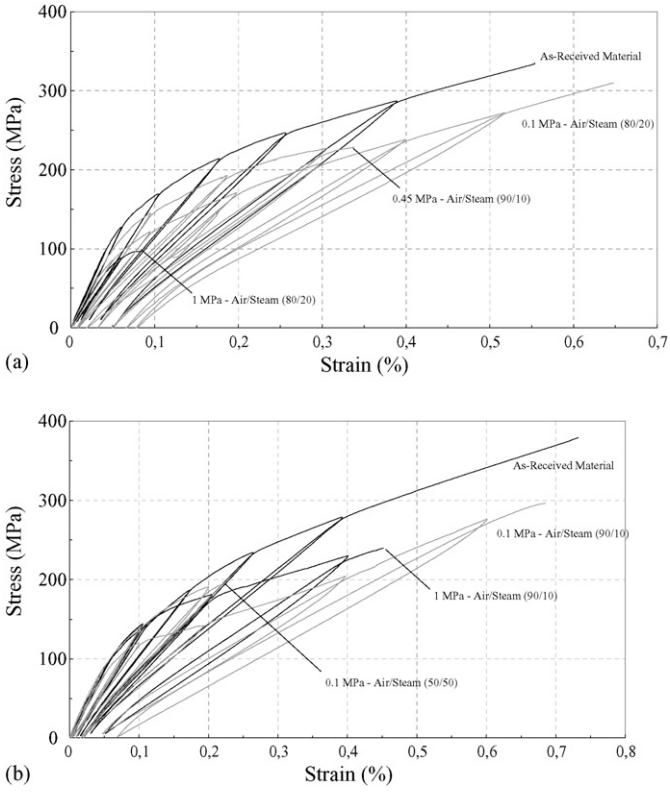

Fig. 7. Stress–strain curves of the C410 specimens of batch 1 (a) and batch 2 (b) obtained at RT after exposure at 1200 °C for 600 h in various environments.

at the edge of the bulk porosities filled with an oxide phase, are observed on the fractured surfaces of the samples aged in high water vapor-pressure environments (Fig. 6). The high steam-pressure exposures affect the ultimate tensile strength (UTS) and the strain to failure of the C410 composites, leading to reductions of 25–70% and 25–80%, respectively (Fig. 5).

The variations of the secant modulus, shown in Fig. 8, are determined from the stress–strain curves at each load–unload loop to highlight the damage progression in the composites. First, the initial modulus of the aged composites has to be compared with the as-received material modulus corresponding to the stress used for the pre-damaging (150 MPa). Thus, the exposed materials have an initial modulus higher than the modulus of the as-received material corresponding to a stress of 150 MPa. This is consistent with the sealing of the pre-damaging cracks with an oxide phase. Nevertheless, increasing the stress results in a decrease of the modulus of the aged composites faster than for the as-received material. This corresponds to a faster damage progression in these aged specimens, certainly associated to local brittle ruptures of few tows. This results in a premature failure except for the materials exposed at low steam-pressure (environments A and B in Fig. 5). The modulus at failure, determined using a linear extrapolation of the measured modulus (dotted lines in Fig. 8), is compared with the theoretical modulus at failure E_{Th}. It is calculated from the following relation:

$$E_{Th} = \frac{1}{2} V_f E_f \quad (10)$$

where V_f is the fiber volume (34%), E_f the fiber modulus at RT (Hi-Nicalon® fiber: 250 GPa) and E_{Th} the theoretical modulus at failure of a 2D woven composite considering that only the fibers, oriented in the direction of the loading axis, bear the load at failure.

The materials exposed in the environments F and C have the lower retained mechanical properties and their extrapolated modulus at failure are significantly higher than the theoretical modulus (Fig. 8). This is consistent with a very fast damage progression and an embrittlement of the composite.

The residual strains after unloading of the composites exposed at low steam-pressure are strongly increased at a stress slightly higher than 100 MPa, by comparison with the as-received materials (Fig. 9). This could be related to the presence of the brittle areas observed on the fractured surfaces. Indeed, brittle rupture areas could occur at a stress of 100–150 MPa. Thus, the load is transferred on the remaining unbroken fibers. This could result in a sudden opening of the cracks with the extension of the debonded length in the non- or less-oxidized areas, enhancing the sliding of the fibers.[22,23] However, the mechanical properties at failure are maintained (Fig. 5). The residual strains after unloading of the strongly damaged composites exposed in the high steam-pressure environments, show low or non-significant variations by comparison with the as-received material (Fig. 9). This is in agreement with their brittle failure (Table 2) certainly caused by the increase of the interfacial shear stress at the fiber/matrix interphase.

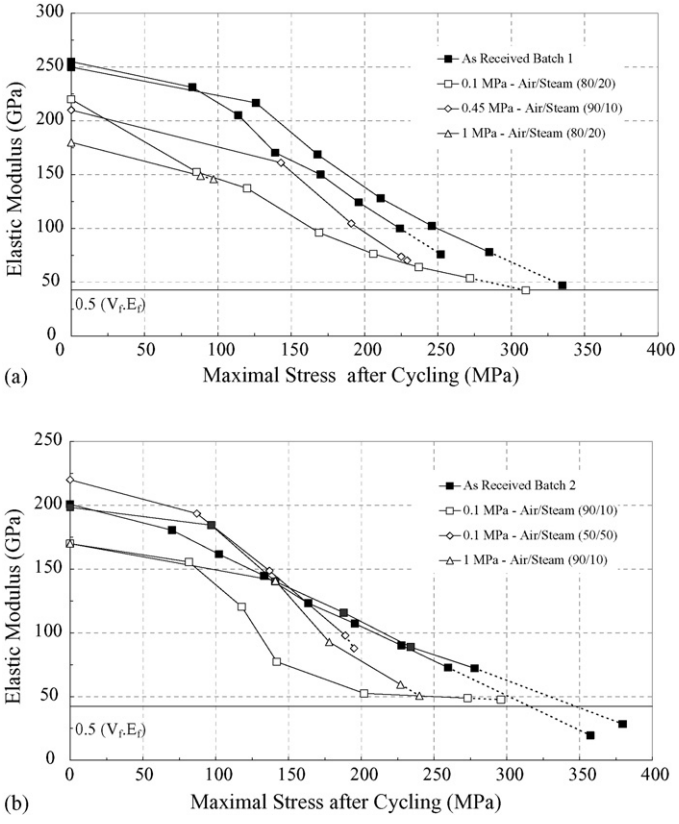

Fig. 8. Damage progression of C410 specimens from batch 1 (a) and batch 2 (b) during tensile cycling at RT after exposures at 600 °C for 600 h in various environments (the dotted lines correspond to the modulus at failure extrapolated from (7)).

4.2. Weight changes

Weight changes of C410 composites after exposures at 1200 °C in various environments for 600 h are reported in Table 2 and shown in Fig. 10. All of the samples show significant weight gains, between 2.5 and 6%, attributed to the formation of an oxide phase generated by the matrix oxidation at the surface and in the bulk. After a time t, which depends on the exposure conditions, the weight gains reach a pseudo-steady state corresponding to the sealing of the seal-coat microcracks and the partial or total filling of the bulk porosities. The weight change kinetics before reaching the steady state can be characterized by weight gain rates obtained from linear regressions (Fig. 11). Fig. 11 shows that high-pressure environments enhance the initial oxidation kinetics, thus reducing the time to achieve the sealing of the composite. Thus, by increasing the total pressure by a factor of 10, the linear weight gain rate is increased four-fold. In the atmospheric pressure environments, increasing steam-pressure results in higher weight gain rates which are comparable, for the air/steam (50/50) gas mixture, to those obtained in high-pressure environments. This is consistent with previous works which showed that the silicon carbide oxidation kinetic is dramatically enhanced in presence of steam[14–16] (the SiC oxidation rate is proportional to P_{H_2O} with a power law exponent of 1). Nevertheless, increasing the water vapor

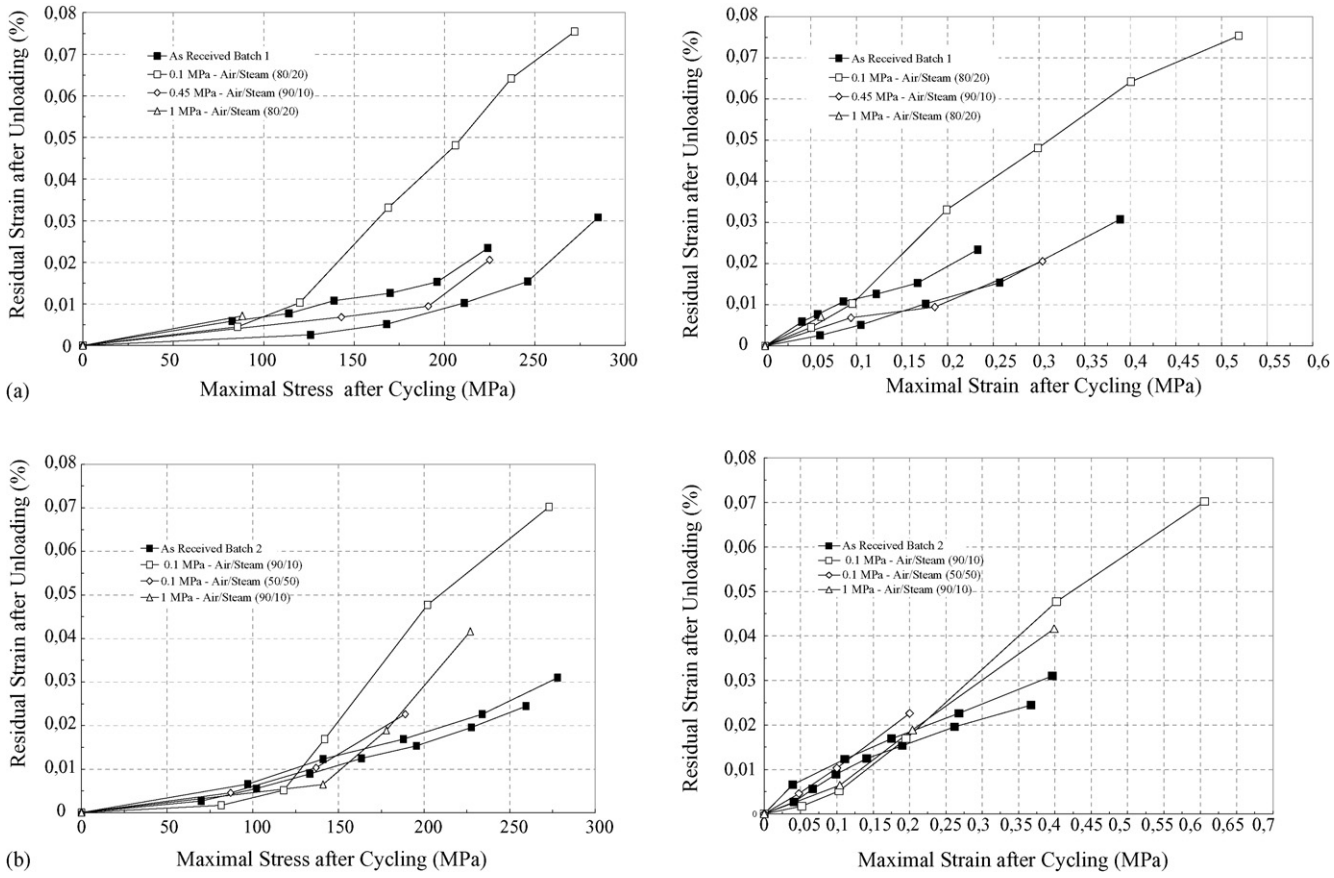

Fig. 9. Variation of the residual strains after unloading of C410 specimens from batch 1 (a) and batch 2 (b) during tensile cycling at RT after exposure for 600 h in various environments.

pressure in high-pressure environments by a factor 2 does not enhance significantly the weight gain rates. This variation of rate is certainly slowed down because of a diffusion controlled regime in which oxidation kinetics are dependent on the rate at which oxygen and water vapor are supplied to the surface.

4.3. Post-exposure observations of C410 composites

All of the exposed C410 specimens were examined in the gage region. The matrix final layer at the surface and in the bulk is SiC. The material can be considered as a complex layered structure of the different constituents SiC, B_4C and Si–B–C which are oxidized in sequence as the oxidation front progresses through the core. Thus, the SiC matrix layers oxidize first followed by the boron components through the pre-damaging cracks and the bulk porosities (Fig. 12). Each layers oxidizes at a different rate according to (i) the reactions (1)–(9) forming gaseous reaction products and glass, (ii) the quantity of generated sealing phase and (iii) the capability of oxygen to diffuse and the volatility of glass which are dependent on its composition. Silica and boria

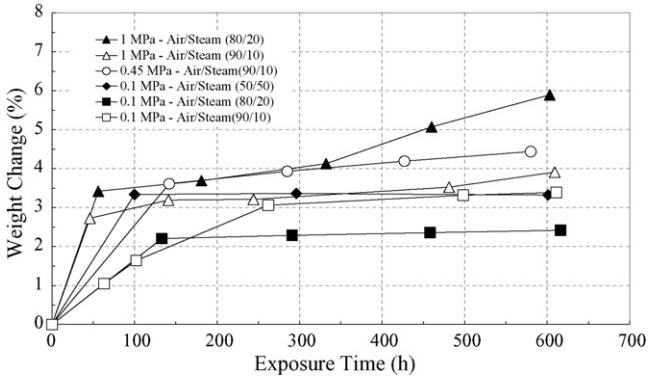

Fig. 10. Weight change kinetics of C410 composites exposed at 1200 °C for 600 h in various environments.

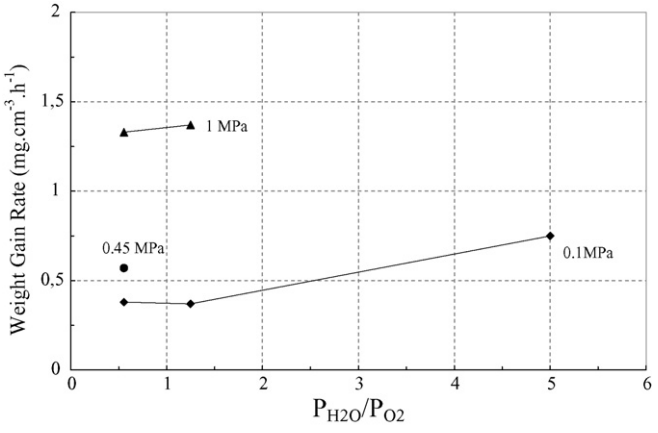

Fig. 11. Linear weight gain rates of C410 composites exposed at 1200 °C for 600 h in various air/steam gas mixtures.

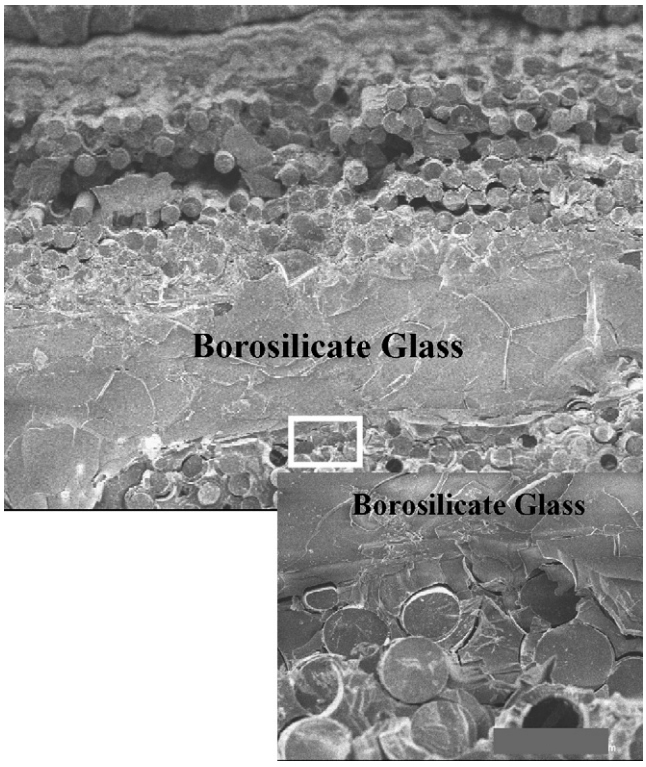

Fig. 12. SEM fracture surface of a C410 specimen exposed in an air/steam (50/50) gas mixture for 601 h at 1200 °C and 0.1 MPa, then tested in tension at RT showing the attacked SiC fibers embedded in a borosilicate glass at the edge of a sealed bulk porosity.

react to form a liquid borosilicate glass, flowing more easily than pure silica, which seals the bulk porosities and the pre-damaging cracks of the seal-coat (Fig. 12). The borosilicate is not protective enough and once the first matrix layer around the fibers is reached, the oxidation of the tows (fiber and PyC interphase) occurs (Fig. 12). The SiC fiber oxidation kinetic can be dramatically enhanced by contact with the boria-containing glass, in agreement with the following reaction[24–26]:

$$x\mathrm{SiC}_{(s)} + y\mathrm{B_2O_{3(l)}} = z\mathrm{B_2O_3} - v\mathrm{SiO_{2(soul)}} + u\mathrm{CO_{(g)}} \qquad (11)$$

The widest damaged areas, characterized by the dissolving of tows with a large amount of fibers embedded in the borosilicate glass, are observed on the composites exposed in high steam-pressure environments (Figs. 12 and 13). These degradations are responsible for the strong decrease of their mechanical properties (environments C and F in Fig. 5). Not only the presence of steam accelerates the oxidation of SiC and boron components, but the high O_2 and $H_2O_{(g)}$ diffusivities through the borosilicate glass further increase the degradation rates of the composites constituents. Thus, in the highest steam-pressure environment (1 MPa—air/steam (80/20)), the exposure for 600 h leads to the total degradation of the seal-coat which is replaced by a thick oxide layer in contact with the fibers (Fig. 13). Impurities present in these industrial composites also increase the oxidation rates, particularly in presence of water vapor. Finally, excessive amounts of gaseous reaction products are formed, creating porosities and resulting in a non-protective borosilicate glass.

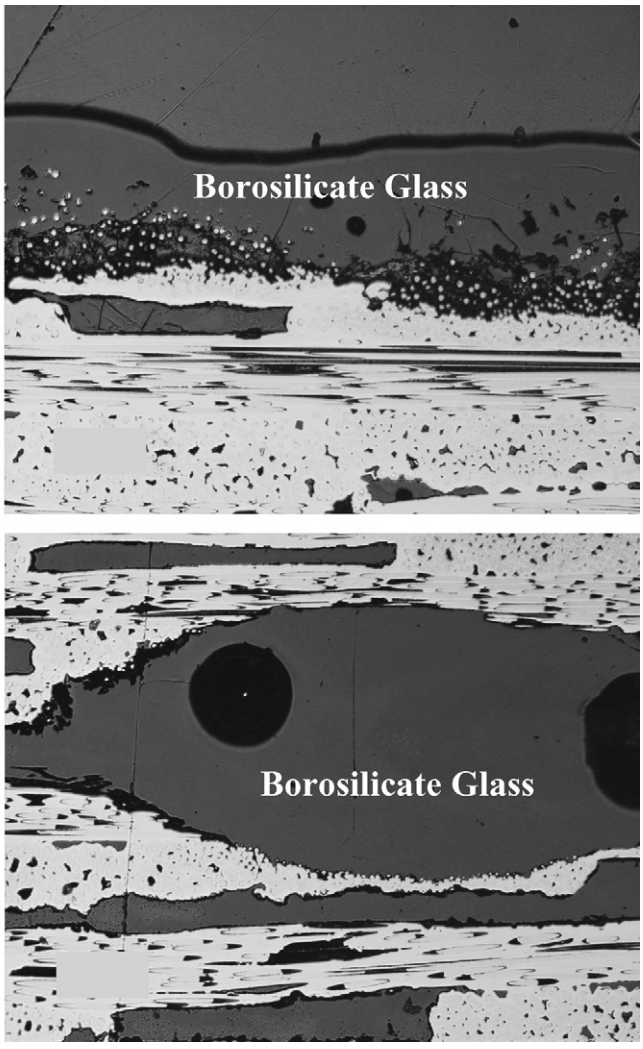

Fig. 13. Polished cross-sections of a C410 composite exposed at 1200 °C and 1 MPa in an air/steam (80/20) gas mixture for 603 h then tested in tension at RT, showing the damages at the surface (a) and in the bulk (b).

4.4. Analysis of the oxides generated

Polished cross-sections in the gage length of the exposed specimens are analyzed by EPMA. The mean compositions of the bulk borosilicate glass are obtained from 40 to 60 measurement points located in several filled bulk porosities (Fig. 14). All of the materials exposed for 600 h contain an oxide phase rich in silica, with a boria molar content ranging from 5 to 20%. The low boria content is due to (i) its high volatility at high temperature in steam environments and (ii) its reaction with SiC to form silica. Thus, the lowest boria content is obtained in the highest steam-pressure environment which caused the more important damages in the material. Nevertheless, the oxide composition in the other environments after 600 h exposure, seems to be not clearly dependent on the total pressure and the water vapor content.

Fig. 15 highlights a localised boria gradient in the glass with a minimal boria content around the fibers attacked. This is due to formation of silica by oxidation of the SiC fibers, highly enhanced by boria (11).

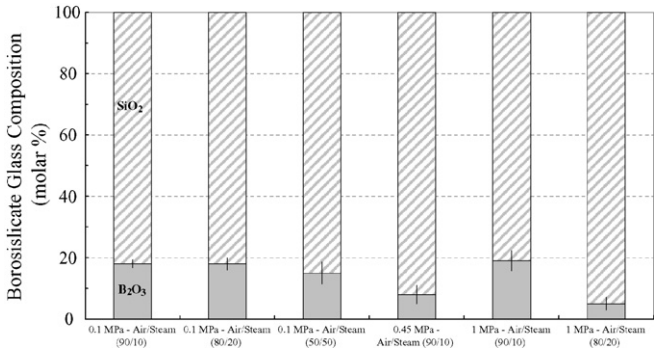

Fig. 14. Mean compositions of the borosilicate glass sealing the bulk porosities of C410 composites exposed for 600 h in various environments at 1200 °C. Results obtained using EPMA.

5. Discussion

5.1. Effect of the total pressure

Fig. 16 shows that increasing the total pressure of the environment leads to a significant reduction of the UTS and strain to failure of the C410 material. Thus, by increasing the total pressure of an air/steam (80/20) gas mixture by a factor of 10, the UTS and strain to failure are divided by 3 and 8, respectively. This can be attributed to the enhancement of oxidation kinetics in high-pressure environments resulting in the increase of the weight gain kinetics (Figs. 10 and 11). Indeed, the borosilicate glass, generated faster and in high quantity, accelerates the oxidation of the silicon carbide in contact (11). This, first increases the matrix oxidation, then the fiber reinforcement consumption during the long times of exposure. Thus, the fiber volume decreases and is replaced by a borosilicate phase which weakens the mechanical properties of C410. Indeed, firstly, diminishing the fiber volume by dissolving of SiC decreases the number of fibers bearing the load and, thus the UTS (Figs. 5 and 16). Secondly, the attacked fibers are embedded in glass (strong fiber/oxide chemical bond at RT) which facilitates the propagation of the matrix cracks and causes the ultimate strain and the UTS to diminish.

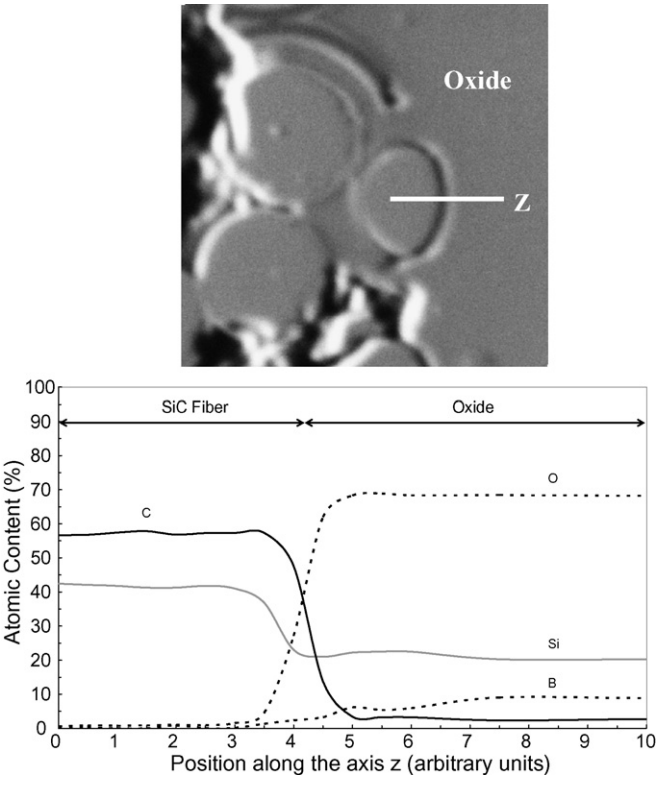

Fig. 15. EPMA line scanning profile (axis *Z*) in a filled bulk porosity of a C410 specimen exposed at 1200 °C and 0.1 MPa for 601 h in an air/steam (50/50) gas mixture.

5.2. Effect of the ratio P_{H_2O}/P_{O_2}

Fig. 16 highlights that, increasing the ratio P_{H_2O}/P_{O_2}, i.e. the water vapor content relatively to the oxygen content, reduces significantly the UTS and strain to failure of the C410 material in both atmospheric pressure and high-pressure environments. Thus, increasing the ratio P_{H_2O}/P_{O_2} by a factor 9 in atmospheric pressure gas mixtures decreases the UTS and the strain to failure by a factor of 1.5 and 3, respectively. These variations are enhanced in high-pressure environments, in agreement with the effect of the total pressure previously described. Thus, UTS and strain to failure diminish by a factor 2.5 and 4 with the only increase of P_{H_2O}/P_{O_2} by a factor 2. It is well known that the presence of water vapor enhances the oxidation kinetic of silicon

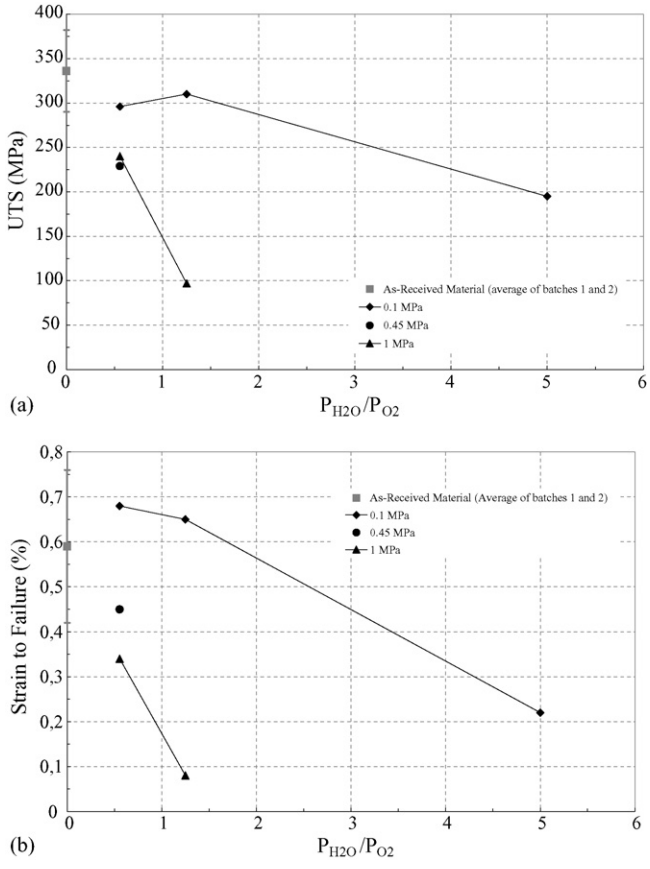

Fig. 16. Effects of the environment on UTS (a) and strain to failure (b) of C410 composites exposed at 1200 °C for 600 h in various air/steam gas mixtures.

carbide at high temperature[14–16] (8). This effect is attributed to the higher solubility of water in the borosilicate glass relatively to oxygen by creation of Si–OH bonds. It is generally agreed that the SiC oxidation rate is proportional to P_{H_2O} with a power law exponent of 1.[15,16] The oxidation of the boron components is also increased in high steam-pressure environments leading to an acceleration of the C410 matrix oxidation kinetic. The faster generation of the liquid boria-containing glass facilitates the silicon carbide dissolving (10), thus the progression of the oxidation front in the bulk composite. This results in (i) an acceleration of the fibers oxidation/dissolving kinetic and (ii) an increase of the amount of fibers strongly bonded together with rigid bridges of glass (or embedded in glass), which cause embrittlement and weakening of the composite (Figs. 5 and 16). The second effect of steam on silicon and boron-based ceramics is the increase of silica and boria volatilities leading to linear material recession rates. It is shown that the linear oxide volatilization and linear recession rates k_l have the following dependence[17–19]:

$$k_l \alpha P_{H_2O} \frac{v^{1/2}}{P_{Tot}^{1/2}} \quad (12)$$

where P_{H_2O} is the water vapor partial pressure (MPa), P_{Tot} the total pressure (MPa) and v the velocity of the gases (m s^{-1}).

Despite the fact that the volatility of B_2O_3 is very important at high temperature and in steam environments,[4–6,8,12,1,3] it is not high enough to avoid the dissolving reaction of SiC (Fig. 13). This can be attributed to (i) the presence of silica which reduces the volatility of B_2O_3 in the borosilicate glass and (ii) the velocity of the gases which is highly decreased in the bulk composite, thus diminishing the volatilization of B_2O_3, in agreement with (12).

5.3. Quantification of the corrosion damages

A theoretical approach, based on the retained mechanical properties (UTS and elastic modulus) obtained at RT, is developed to quantify the corrosion damages in the composite (Appendix A). The results, shown in Fig. 17, show that the materials aged at low steam-pressure are less affected than the composites tested at high steam-pressure. In agreement with the morphological analyses, the highest fiber volume consumption associated with the highest formed oxide volume are obtained in the high steam-pressure environments. The theoretical approach is not applied to the composite exposed at atmospheric pressure in the air/steam (50/50) gas mixture because its modulus is higher than the as-received material one (not pre-damaged). This could be due to a large amount of fibers strongly bonded together by the borosilicate glass. Finally, the measurement of the strain could be slightly under-estimated because of the un-homogeneous damage across the section (only one spring-loaded clip on-gauge used).

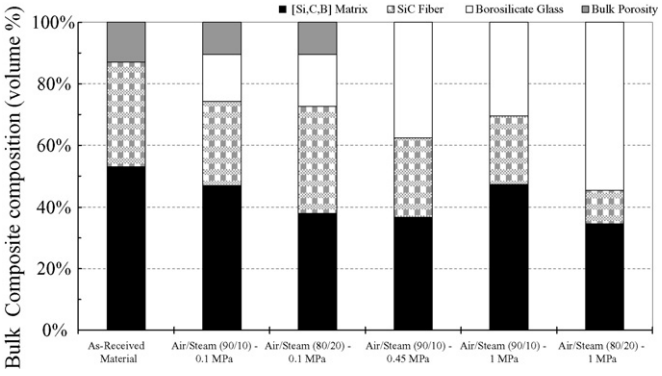

Fig. 17. Quantification of the corrosion damages in the C410 material exposed at 1200 °C for 600 h in various environments, based on a theoretical approach and the post-exposure mechanical properties.

6. Conclusions

The study of $SiC_{(f)}$/[Si, C, B]$_{(m)}$ specimens exposed for periods up to 600 h at 1200 °C in slow-flowing air-steam gas mixtures, in an atmospheric pressure furnace and in a high-pressure furnace, have shown several results. The material shows no significant degradation of its retained mechanical properties (strength and fracture strain) after exposures at atmospheric pressure for up to 600 h in air-steam (90/10) and (80/20) gas mixtures. However, for a 600 h exposure in a 50% steam-containing environment at atmospheric pressure, the material losses over 40% of its strength and 70% of its strain to failure. In an air-steam (80/20) gas mixture at 1 MPa, strength and fracture strain reductions higher than 65 and 80%, respectively, are observed after exposure for up to 600 h. Steam-pressure has a key role in the mechanism of degradation at 1200 °C and similar damages observed in high-pressure environments with low-steam-content can be obtained in atmospheric pressure environments with high-steam-content. Microstructural evidence of the damages includes (i) the generation of a borosilicate glass sealing the bulk porosities, (ii) the multi-layered matrix oxidation and (iii) the oxidation/dissolving of the fibers which are strongly bonded together and embedded in the solid glass at RT. High steam-pressure environments enhance the matrix oxidation and the generation of a liquid borosilicate glass through the pre-damaging cracks and the bulk porosities. B_2O_3, contained in the borosilicate (5–20% molar after 600 h exposures), may first react with SiC matrix layers to form silica before reaching the fibers and causes embrittlement and weakening of the composites. Moreover, under mechanical loading, microcracks can open or connect initially closed bulk porosities, thus enhancing the diffusion of oxygen and steam through the material. This phenomenon should be taken into account to predict the durability of $SiC_{(f)}$/[Si, C, B]$_{(m)}$ composites.

The service conditions of an aeronautic engine including the combination of high temperatures and high steam-pressures, possess a high potential for severe degradation of the mechanical properties in combustor components made of $SiC_{(f)}$/[Si, C, B]$_{(m)}$ composites. Nevertheless, the combustor components made of C410 material possess thicker seal-coat than the machined dog-bone specimens used in this study, thus increasing their life durability. Environmental barrier coatings may be required for long-term use of $SiC_{(f)}$/[Si, C, B]$_{(m)}$ materials in high temperature combustion environments.

Acknowledgements

This work has been supported by the Centre National de la Recherche Scientifique (CNRS) and Snecma Propulsion Solide (SPS) through a grant given to L. Quémard. The authors are grateful to M. Cataldi, J. Lamon and G. Falguieres for fruitful discussions, SPS for production of the samples, R. Bouvier for assistance with corrosion tests, P. Ophele and F. Labarriere for assistance with mechanical tests and M. Lahaye for assistance with EPMA analyses.

Appendix A. Quantification of the corrosion damages: a theoretical approach

This approach is based on the comparison of the UTS and the elastic modulus at room temperature of the exposed composites with the as-received ones. The model assumes that the fibers oriented in the direction of the loading axis and not bonded together with rigid bridges of glass at RT, bear the load at failure. Thus, the reduction of the strength of the materials exposed during a time t can be related to the volume of the remaining non-bonded fibers, V_f^t, using the following equation:

$$V_f^t = \left(\frac{\sigma_r^t}{\sigma_r^0}\right) V_f^0 \tag{A.1}$$

where σ_r^t is the strength at failure of the material after the exposure time t, σ_r^0 and V_f^0, respectively, the strength at failure and the fiber volume of the as-received material (34%).

The elastic modulus at RT of the as-received material (E_c^0) and of the aged composite (E_c^t) can be described, in first approximation, by the following law of mixtures:

$$E_c^0 = E_f^0 V_f^0 + E_m^0 V_m^0 \tag{A.2}$$

$$E_c^t = E_f^0 V_f^t + E_m^t V_m^t \tag{A.3}$$

where E_f^0 is the fiber modulus at RT (Hi-Nicalon® fiber: 250 GPa), E_m^0 and E_m^t the matrix modulus at RT of the as-received material and of the aged composite, V_m^0 and V_m^t, respectively, the matrix volume of the as-received material and of the aged composite.

The corrosion tests at 1200 °C lead to a matrix oxidation. After an exposure time t, the whole matrix can be described as a juxtaposition of the non-oxidized matrix and the oxide phase. Thus, the modulus E_m^t can be determined using the following law of mixture:

$$E_m^t = E_m^0 V_{m,\text{non-ox}}^t + E_{ox} V_{ox} \tag{A.4}$$

where $V_{m,\text{non-ox}}^t$ is the matrix volume non-oxidized after the exposure time t, E_{ox} and V_{ox}, respectively, the modulus and the volume of the oxide phase in the bulk aged composite. According to the composition of the oxide phase, E_{ox} is considered equal to 80 GPa.

The following relation can be written, assuming that the generated oxide phase contains a low porosity which can be neglected:

$$V_{m,\text{non-ox}}^t + V_{ox} = 1 \tag{A.5}$$

The combination of (A.4) and (A.5) allows to write the following relation:

$$V_{m,\text{non-ox}}^t = \frac{E_m^t - E_{ox}}{E_m^0 - E_{ox}} \tag{A.6}$$

The matrix volume of the aged composite is given by the following relation:

$$V_m^t = 1 - V_f^t - (1 - F_p^t)V_p^0 \tag{A.7}$$

where V_p^0 is the total volume of the porosities contained in the as-received material (≈13%) and F_p^t is the volume fraction of the filled porosities.

The combination of the relations (A.1)–(A.3), (A.6) and (A.7) allows to write (A.8):

$$V_{m,\text{non-ox}}^t = \frac{[((E_c^t - E_f^0)((\sigma_r^t/\sigma_r^0)V_f^0))(1 - (\sigma_r^t/\sigma_r^0)V_f^0 - (1 - F_p^t)V_p^0)^{-1}] - E_{ox}}{[(E_c^0 - (E_f^0 V_f^0))/V_m^0] - E_{ox}} \tag{A.8}$$

The non-oxidized matrix volume in the composite $V_{m_c,\text{non-ox}}^t$ is obtained by the following relation:

$$V_{m_c,\text{non-ox}}^t = V_m^t V_{m,\text{non-ox}}^t \tag{A.9}$$

The combination of the relations (A.1), (A.7)–(A.9) allows to obtain the final expression of $V_{m_c,\text{non-ox}}^t$ after exposures in corrosive environments:

$$V_{m_c,\text{non-ox}}^t = \frac{[((E_c^t - E_f^0)((\sigma_r^t/\sigma_r^0)V_f^0))(1 - (\sigma_r^t/\sigma_r^0)V_f^0 - (1 - F_p^t)V_p^0)^{-1}] - E_{ox}}{[(E_c^0 - (E_f^0 V_f^0))/V_m^0] - E_{ox}} \left(1 - \left(\frac{\sigma_r^t}{\sigma_r^0}\right) V_f^0 - (1 - F_p^t)V_p^0\right) \tag{A.10}$$

The volume of the oxide in the composite after an exposure time t in a high steam-pressure environment, V_{ox}, is calculated using the following relation:

$$V_{ox} = 1 - V_f^t - V_{m_c,\text{non-ox}}^t \tag{A.11}$$

The expression of V_{ox} is obtained by combination of the relations (A.1), (A.10) and (A.11):

$$V_{ox} = 1 - \left(\frac{\sigma_r^t}{\sigma_r^0}\right) V_f^0 - (1 - F_p^t)V_p^0 - \frac{[((E_c^t - E_f^0)((\sigma_r^t/\sigma_r^0)V_f^0))(1 - (\sigma_r^t/\sigma_r^0)V_f^0 - (1 - F_p^t)V_p^0)^{-1}] - E_{ox}}{[(E_c^0 - (E_f^0 V_f^0))/V_m^0)] - E_{ox}} \times \left(1 - \left(\frac{\sigma_r^t}{\sigma_r^0}\right) V_f^0 - (1 - F_p^t)V_p^0\right) \tag{A.12}$$

In high steam-pressure environments, the morphological observations showed that all of the bulk porosities are filled with an oxide phase. Thus, F_p^t is equal to 1. At the opposite, in low steam-pressure environments, the volume fraction of the bulk porosities of the as-received material which are filled with the glass is estimated at 20% approximately. Thus, F_p^t is equal to 0.2.

References

1. Lamouroux, F., Pailler, R., Naslain, R. and Cataldi, M., French Patent No. 95 14843, 1995.
2. Vandenbulcke, L. and Goujard, S., Multilayer systems based on B, B_4C, SiC and SiBC for environmental composite protection. *Prog. Adv. Mater. Mech.*, 1996, 1198–1203.
3. Bouillon, E., Spriet, P., Habarou, G., Louchet, C., Arnold, T., Ojard, G. C. *et al.*, Engine test and post engine test characterization of self sealing ceramic matrix composites for nozzle applications in gas turbine engines, *ASME TURBO EXPO 2004. Power for Land, Sea and Air*. Vienna, Austria, 2004. ID GT-2004-53976.
4. Martin, X., Rebillat, F. and Guette, A., Oxidation behavior of a multilayered (Si–B–C) ceramic in a complex atmosphere $N_2/O_2/H_2O$. *High Temp. Corros. Mater. Chem.*, in press.
5. Rebillat, F., Martin, X. and Guette, A., Kinetic oxidation laws of boron carbide in dry and wet environments. In *Proceedings of High Temperature Ceramic Matrix Composites 5 (HTCMC5)*, ed. M. Singh, R. Kerans, E. Lara-Curzio and R. Naslain. American Ceramic Society, Westerville, OH, USA, 2004, pp. 321–326.
6. Quémard, L., Martin, X., Rebillat, F. and Guette, A., Thermodynamic study of B_2O_3 reactivity in $H_2O_{(g)}N_{2(g)}/O_{2(g)}$ atmospheres at high pressure and high temperature. In *Proceedings of High Temperature Ceramic Matrix Composites 5 (HTCMC5)*, ed. M. Singh, R. Kerans, E. Lara-Curzio and R. Naslain. American Ceramic Society, Westerville, OH, USA, 2004, pp. 327–332.
7. Farizy, G., *Mécanisme de fluage sous air de composites SiC_f/$SiBC_m$ à matrice auto-cicatrisante*. Ph.D. thesis, University of Caen, 2002.
8. Viricelle, J. P., Oxidation behaviour of a multi-layered ceramic matrix composite $(SiC)_f/C/(SiBC)_m$. *Compos. Sci. Technol.*, 2001, **61**, 607–614.
9. Quemard, L., Rebillat, F., Guette, A., Tawil, H. and Louchet-Pouillerie, C., Corrosion behavior of a SiC fiber reinforced self sealing matrix composite at intermediate temperature and in a high pressure steam environment, in press.
10. Bouillon, E., Abbé, F., Goujard, S., Pestourie, E. and Habarou, G., Mechanical and thermal properties of a self sealing matrix composite and determination of the lifetime duration. *Ceram. Eng. Sci. Proc.*, 2000, **21**(3), 459–467.
11. Bouillon, E., Lamouroux, F., Baroumes, L., Cavalier, J. C., Spriet, P. and Habarou, G., An improved long life duration CMC for jet aircraft engine applications, *ASME TURBO EXPO 2002*. Amsterdam, The Netherlands, 2002. ASME ID GT-2002-30625.
12. Jacobson, N., Farmer, S., Moore, A. and Sayir, H., High temperature oxidation of boron nitride. I. Monolithic boron nitride. *J. Am. Ceram. Soc.*, 1999, **82**(2), 393–398.
13. Jacobson, N., Farmer, S., Moore, A. and Sayir, H., High temperature oxidation of boron nitride. II. Boron nitride layers in composites. *J. Am. Ceram. Soc.*, 1999, **82**(6), 1473–1482.
14. Opila, E. J. and Hann Jr., R. E., Paralinear oxidation of CVD SiC in water vapor. *J. Am. Ceram. Soc.*, 1997, **80**(1), 197–205.
15. Opila, E. J., Oxidation and volatilisation of silica formers in water vapor. *J. Am. Ceram. Soc.*, 2003, **86**(8), 1238–1248.
16. Opila, E. J., Oxidation kinetics of chemically vapor-deposited silicon carbide in wet oxygen. *J. Am. Ceram. Soc.*, 1994, **77**(3), 730–736.
17. Opila, E. J., Fox, D. S. and Jacobson, N. S., Mass spectrometric identifictaion of $Si–O–H_{(g)}$ species from the reaction of silica with water vapor at atmospheric pressure. *J. Am. Ceram. Soc.*, 1997, **73**(12), 1009–1012.
18. Robinson, R. C. and Smialek, J. L., SiC recession caused by SiO_2 scale volatility under combustion conditions. I. Experimental results and empirical model. *J. Am. Ceram. Soc.*, 1999, **82**(7), 1817–1825.
19. Opila, E. J., Smialek, J. L., Robinson, R. C., Fox, D. S. and Jacobson, N. S., SiC recession caused by SiO_2 scale volatility under combustion conditions. II. Thermodynamics and gaseous diffusion model. *J. Am. Ceram. Soc.*, 1999, **82**(7), 1826–1834.
20. Yuri, I., Hisamatsu, T., Etori, Y. and Yamamoto, T., Degradation of silicon carbide in combustion gas flow at high temperature and speed. In *Proceedings of ASME TURBOEXPO 2000*, 2000.
21. Quemard, L., Rebillat, F., Guette, A. and Tawil, H., Development of an original design of high temperature–high pressure furnace. In *Proceedings of High Temperature Ceramic Matrix Composites 5 (HTCMC5)*, ed. M. Singh, R. Kerans, E. Lara-Curzio and R. Naslain. American Ceramic Society, Westerville, OH, USA, 2004, pp. 543–548.
22. Corne, P., Rechiniac, C. and Lamon, J., Approche des propriétés de l'interface fibre-matrice dans les composites à matrice céramiques: résistance à la décohesion. In *Proceedings of JNC 8*, ed. O. Allix, J. P. Favre and P. Ladeveze. AMAC, Paris, 1992, pp. 213–223.
23. Lamon, J., Rebillat, F. and Evans, A., Assessment of a microcomposite test procedure for evaluating constituent properties of ceramic matrix composite. *J. Am. Ceram. Soc.*, 1995, **78**(2), 401–405.
24. Ogbuji, L. U. J. T., A pervasive mode of oxidative degradation in a SiC–SiC composite. *J. Am. Ceram. Soc.*, 1998, **81**(11), 2777–2784.
25. Ogbuji, L. U. J. T., Oxidative pest degradation of Hi-Nicalon/BN/SiC composite as a function of temperature and time in the burner rig. In *Proceedings of Cocoa Beach*, 1999.
26. Yun, H. M., Tensile behavior of as-fabricated and burner rig exposed SiC/SiC composites with Hi-Nicalon Type S Fibers. In *Proceedings of 26th International Cocoa Beach Conference on Advanced Ceramic Composites*, 2002.